The Distribution of Freely Suspended Particles at Microfluidic Bifurcations

Brian W. Roberts and W. L. Olbricht
School of Chemical and Biomolecular Engineering, Cornell University, Ithaca, NY 14853

DOI 10.1002/aic.10613
Published online September 1, 2005 in Wiley InterScience (www.interscience.wiley.com).

The distribution of freely suspended particles in low Reynolds number, pressure-driven flow through bifurcations of microfluidic channels is measured experimentally. A bifurcation is a point where a channel splits into multiple channels. The partitioning of particles at microfluidic bifurcations differs from the partitioning of fluid, which can, in principle, be exploited to direct the particles along preferred paths in microfluidic devices or to prevent particles from entering certain microchannels. Experiments are conducted to examine effects of the angles between branches of the bifurcation and the microchannel cross-sectional shape on particle partitioning. Furthermore, effects of multiple bifurcations in series on the partitioning of particles also are examined. Under certain conditions, the particles can be completely segregated from the suspending fluid, which could be used as a flow-through filter for microfluidic devices. © 2005 American Institute of Chemical Engineers *AIChE J,* 52: 199–206, 2006
Keywords: separations, microfluidics, particulates, filtration, microfabrication

Introduction

Microfluidic systems offer important potential advantages in chemical processing, including precise control of fluid motion, controlled interactions with solid surfaces, rapid response times, small sample volumes, and minimization of wastes and unwanted by-products. To take advantage of these benefits, efficient ways must be found to move liquids precisely through complicated networks of micron-sized channels. In some applications, the liquid may contain freely suspended particles that move through the microchannels with the liquid. Depending on the application, the particles may be rigid particles, immiscible liquid drops, vesicles, or biological cells. Processing liquids that contain freely suspended particles in small channels poses special challenges. The particles can foul sensors embedded within the microfluidic circuit, interfere with flow control components such as gates and valves, and perturb the distribution of liquid flow rates among the various channels in a microfluidic network. Therefore, controlling the motion of freely suspended particles is essential for processing multiphase systems in microfluidic devices.

The motion of freely suspended particles and immiscible liquid drops in channels is the subject of a rich literature in hydrodynamics. Because of the small size of the channels, many microfluidic devices operate in the low Reynolds number limit. It seems reasonable to ask whether knowledge of particle motions in low Reynolds number channel flow can be exploited in device design to control the motion of particles in complex microfluidic circuits. It may be possible, for example, to control the distribution of particles among the microchannels, to confine particles to preferred paths through a network of microchannels, to classify the particles based on size, to deliver the particles to certain sites in the network, or to remove them altogether when they are unwanted impurities or contaminants. Although the paths that particles take in a network could be controlled by continuously adjusting local flow rates so that the particles are carried into selected channels, making many such adjustments in situ is difficult in microfluidic devices, especially for networks with many channels and particles.

For low Reynolds numbers, the motions of liquid and freely suspended particles are determined completely by the channel geometry and the way the channels are connected to each other.

Correspondence concerning this article should be addressed to W. L. Olbricht at wlo@cheme.cornell.edu.

Therefore, it may be possible to control the paths particles take in microfluidic networks simply by making judicious choices of microchannel geometry and of the ways that the channels are arranged into networks. Then, the flow that drives the particles through the network could be used to shunt the particles in preferred directions in the network without making adjustments to flow rates or imposing some other active control mechanism. Because this method of controlling the particles would depend only on the microchannel geometry, the method may be more amenable to scale-up than methods that require active control of local flow rates or pressures in a microfluidic network.

One of nature's primordial microfluidic systems is the mammalian microcirculation—the part of the vasculature composed of networks of interconnected capillaries. Studies of blood cell motion in the microcirculation have shown that the distribution of the cells among the capillaries in a network can be strongly inhomogeneous. Some capillaries may contain a relatively large number of cells, whereas nearby capillaries contain few or no cells. The distribution of cells among the capillaries in the microcirculation is influenced by a variety of factors, including the way that cells move through bifurcations. A *bifurcation* is simply a point where a capillary splits into two capillaries. Experiments show that the partitioning of cells at a capillary bifurcation differs from the partitioning of volume (cells + fluid) at the bifurcation.[1-9]

These results have been confirmed by model experiments[9-12] and theoretical studies[13-16] that use rigid spheres or other particles in place of blood cells. The results show that when the fraction of flow entering one of the downstream branches of a bifurcation exceeds some critical value, all of the particles enter that branch, even though the other downstream branch receives a portion of the suspending liquid. The distribution of particles between the two downstream branches is affected by the size of the particle relative to the size of the capillary tubes composing the bifurcation, by the bifurcation geometry (especially the angles between branches of the bifurcation), and the volume fraction of freely suspended particles.

Most of the experiments have focused on bifurcations composed of branching tubes with circular cross sections. However, the cross sections of channels in microfluidic devices are usually rectangular because of the nature of microfabrication processes. The shape of the channel cross section can influence particle motions, which may, in turn, affect the distribution of particles at bifurcations. Particle trajectories can be difficult to determine from solutions of the appropriate equations of motion because the flow is fully three-dimensional; many trajectories have to be computed and some trajectories bring particles very close to the channel walls.

Therefore, we have carried out a series of experiments to measure the distribution of particles at bifurcations composed of microfluidic channels. We consider cases where the particles are sufficiently large and the suspending liquid is sufficiently viscous that Brownian motion is unimportant. Furthermore, nonhydrodynamic forces between the particles and the channel walls, such as electrostatic or van der Waals forces, are negligible. Under these conditions, particle motions and partitioning at bifurcations are determined completely by hydrodynamic forces. We examine effects of the channel cross-sectional aspect ratio and effects of multiple bifurcations in series on the distribution of freely suspended particles, and we compare results for microchannels with similar results obtained in much larger channels. The results of the experiments are used to illustrate how particle partitioning at bifurcations can be used to control the way that particles move through microfluidic networks.

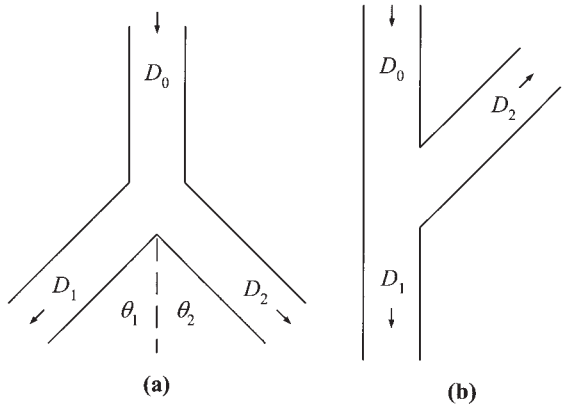

Figure 1. Two bifurcations studied in the experiment.

(a) Y-shaped bifurcation with $\theta_1 = \theta_2 = 45°$; (b) oblique bifurcation with $\theta_1 = 0°$ and $\theta_2 = 135°$. Arrows indicate the direction of flow. In all cases in this report, the widths of the channel branches D_0, D_1, and D_2 are identical.

Experimental

Bifurcation geometries

The geometries of the microfluidic bifurcations are shown in Figure 1. Liquid flows toward the bifurcation through a single inlet branch and away from the bifurcation in two outlet branches, as indicated by the arrows. All three branches lie in the same plane, so that the overall geometry of the bifurcation is determined simply by the angles that the two outlet branches make with respect to the inlet branch. Figure 1a shows a Y-shaped bifurcation in which the downstream branches are symmetric with respect to the inlet; Figure 1b shows an oblique bifurcation where one downstream branch is collinear with the inlet branch, whereas the other outlet branch makes an angle of 135° with respect to the inlet branch. The oblique geometry is used in this study because it was shown in large-scale experiments to be particularly effective at separating particles from fluid.

The dimensions of the channel cross sections were identical for all three branches of the bifurcation in every case. Two channel cross-sectional shapes were tested: a square channel with dimensions of 100×100 μm and a rectangular channel with width of 100 μm and depth of 200 μm.

To test the effects of having several bifurcations in series on particle distributions, the microfluidic network shown in Figure 2 was used. This geometry was chosen so that every path the particles can take through the network contains two bifurcations in series: a Y-shaped bifurcation followed by an oblique bifurcation.

Dimensional analysis and parameters of the experiment

Once the geometry of the bifurcation is specified as in Figure 1, dimensional analysis shows that the trajectory of a neutrally buoyant sphere with radius R through a bifurcation of a rectangular channel with width a and depth b depends on the

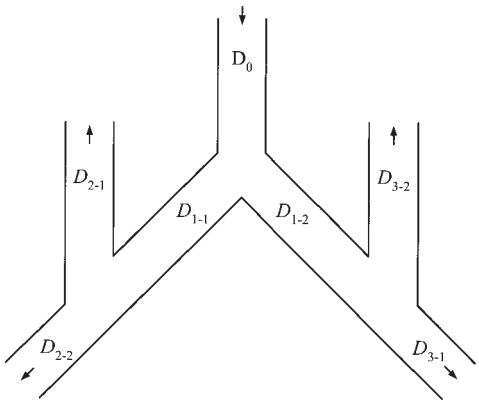

Figure 2. Multiple bifurcation apparatus.

Arrows indicate direction of flow. Each path through the device consists of a Y-bifurcation and an oblique bifurcation in series. All channel widths are equal. $\theta_{1-1} = \theta_{1-2} = 45°$; $\theta_{2-1} = 135°$; $\theta_{2-2} = 0°$; $\theta_{3-1} = 0°$; $\theta_{3-2} = 135°$

following dimensionless parameters: a/b, the aspect ratio of the channel cross section; $\lambda = R/a$, the dimensionless particle size; the Reynolds number in the inlet and downstream channels; the ratio of volumetric flow rates in the two downstream branches of the bifurcation; and the lateral position of the particle in the inlet channel as it approaches the bifurcation. The Reynolds number in this study is always much smaller than unity, which means that its exact value does not affect the trajectories of particles or the partitioning of particles at a bifurcation. Because the volumetric flow rate in the inlet channel and the viscosity of the suspending liquid appear only in the Reynolds number, which is asymptotically small, particle trajectories through a bifurcation are not affected by the flow rate in the inlet channel or the fluid viscosity. Therefore, for a given bifurcation, and for a uniform suspension of particles of fixed size that are randomly distributed in the inlet channel, particle partitioning depends only on the relative flow rates in the downstream branches.

A goal of the present study is to compare results obtained in microfluidic channels with data obtained in "scaled-up" experiments involving channels with much larger dimensions. Studies of particle partitioning in bifurcations of rectangular channels with dimensions on the order of millimeters showed that an effective separation was achieved for a dimensionless particle size λ of 0.77, but that the effectiveness of the separation decreased with decreasing λ. Therefore, a comparable value of λ is used in the present study.

Microfabrication

The microfluidic channels and bifurcations were fabricated in thermoplastic substrates using hot embossing. The process starts by fabricating a master, which contains raised features where channels are desired in the final device. The features of the master are then embossed into a plastic. Although masters are usually fabricated from silicon, the masters in this experiment were fabricated from SU-8, a photoepoxy. Fabricating masters from plastic avoids processing metals, which can be a time-consuming and difficult step in constructing a microfluidic device.

Discs (diameter 4 in.) of 1/8-in. thick aluminum (aluminum alloy 6061; McMaster Carr, Chicago, IL) were polished with 400 grit sandpaper, cleaned with detergent, rinsed with deionized water, and baked on a 200°C hot plate for 1 h to dehydrate the surface, which promotes adhesion of SU-8 to the surface.

The discs were rinsed with isopropanol and dried. Then, 4 mL of SU-8 50 (Microchem, Newton, MA; www.microchem-.com) was spun (300 rpm/s acceleration to 1300 rpm and maintained for 30 s) onto the surface of the disc to form a layer about 100 μm thick. Discs were then covered with a crystallizing dish to prevent dust contamination and baked on a level hot plate (10 min at 65°C, followed by 30 min at 95°C); discs were rotated 180° during baking to ensure the SU-8 layer was uniform in thickness. The entire surface of the SU-8 layer was exposed to UV light (365 nm), baked again on the hot plate (3 min at 65°C, followed by 10 min at 95°C), and finally hard baked for 15 min at 200°C to enhance crosslinking.

A second layer of SU-8 was spun directly on top of the first layer. The thickness of the second layer was equal to the desired feature height. The disc was then covered and the two-step baking procedure described above was repeated. Bake times and temperatures were determined from the manufacturer's specifications for the chosen thickness of the second SU-8 layer. For example, for a second layer with a thickness of 50 μm, the bake times were 3 min at 65°C followed by 10 min at 95°C. Using two layers of SU-8 helps to mitigate thermal incompatibility between the SU-8 and the aluminum substrate. The first layer helps distribute thermal stresses and provides a chemically identical, smooth surface for the second SU-8 layer, which promotes adhesion of the layers. Additionally, the smooth, level surface of the first layer eliminates the need to fine polish the aluminum surface.

The SU-8 composite was then covered with a chrome mask that contained the desired feature pattern for the master. The disc and mask were mounted in a contact aligner (Hybrid Technology Group System III-HR) to ensure proper planarization and hard contact. The assembly was then exposed to UV-light for a time that was determined from the manufacturer's specifications. For example, the exposure time was 65 s at 405 nm for a 100-μm layer. After exposure, the mask was removed, the disc was baked for the prescribed time, and the assembly was cooled to room temperature. The exposed layer was developed in an acetate-based SU-8 developer (Microchem). The developer removed the portions of the second layer that were not exposed to UV light, leaving raised features wherever the mask allowed exposure of the SU-8 layer. The master was then rinsed in isopropanol, blown dry, and hard baked for 15 min at 200°C.

The SU-8 master was strapped onto the bottom plate of an embossing press. A 1/8-in. thick disc of polycarbonate was mounted onto the top plate of the press and held in place by a vacuum applied through a recessed ring in the top plate. The SU-8 master and polycarbonate were brought into close proximity and heated to a temperature that was between 15 and 20°C above the glass-transition temperature (T_g) of the polycarbonate (175°C). They were then pressed together at a pressure of 4 $\pm$ 0.5 MPa. Immediately, the embossing press was water cooled so that the temperature decreased at a rate between 5 and 10°C/min until the temperature of the press was 10°C below T_g (140°C). Figure 3 shows a scanning electron micrograph of an example SU-8 master and the embossed

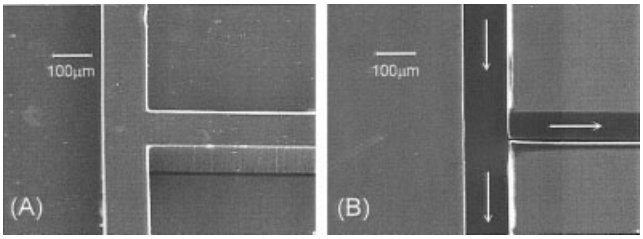

Figure 3. Scanning electron micrograph (SEM) images of 100 × 100-μm T-shaped bifurcation.

(A) SU-8 Master; (B) polycarbonate (PC) part. Arrows illustrate the flow direction in the microfluidic channel in (B).

channels for a T-shaped bifurcation. The arrows illustrate the flow direction in the finished part.

After embossing, each chip was cut from the larger thermoplastic disc and a #56 bit was used to drill ports for the fluid and particles to flow into and out of the chip. The chips were then turned over, and a small countersink was drilled to remove any burrs on the hole and to provide a tapered fit to secure tubing connections.

Apparatus

To seal the microchannels, a silicone rubber gasket was produced by compressing clear silicone rubber adhesive/sealant (RTV 108, General Electric Co. Silicone Products, Waterford, NY) between two 1/4-in. thick polymethylmethacrylate (PMMA) sheets and baking the assembly in a 70°C vacuum oven overnight. The resulting gasket was then placed between the microfluidic chip and a piece of PMMA. The gasket was removable so that the chip could be disassembled, cleaned, and reassembled between experimental runs. The chip housing was mounted under a stereomicroscope (SV8, Carl Zeiss, Oberkochen, Germany), which was equipped with a CCD camera, video timer, and recorder.

Each outlet of the bifurcation was connected through flexible tubing to a syringe in a syringe pump. The pump operated in withdrawal mode, and the relative flow rates in the two downstream branches of the bifurcation were varied by changing the relative sizes of the two syringes. The syringe plungers were withdrawn at the same speed, but the different syringe diameters produced different volumetric flow rates in the two downstream branches. A gel-loading tip was placed at the entrance of the inlet branch to serve as a reservoir for the suspension. Flow rates in the downstream branches were deduced by weighing the syringes before and after a run to determine the amount of fluid that passed through each branch during an experiment.

Flexible, 20-gauge Teflon® needles were fitted to the end of each syringe (catalog no. B-NE-020, Small Parts, Inc., Miami Lakes, FL). The needles could be connected directly to the chip, but in most cases they were connected to the chip with 20-gauge polytetrafluoroethylene thin walled tubing (Small Parts, catalog no. B-STT-20) and slip-on connectors (Small Parts, catalog no. B-TC-20 or B-TCY-20).

Materials

The fluid used in the experiment consisted of a neutrally buoyant suspension of rigid particles in a liquid. The particles were 80-μm rigid spheres (79.6 ± 1.0 μm; catalog no. 4280A, Duke Scientific Corp., Palo Alto, CA). The spheres are supplied from the manufacturer in an aqueous solution. To make the spheres neutrally buoyant, glycerin that was filtered through a 0.45-μm syringe filter to remove contaminants was added to the suspension. A mixture of 19.8 wt % filtered glycerin and 80.2 wt % microsphere solution gave a neutrally buoyant suspension.

Because the chip was cleaned after each run, it had to be primed with fluid at the start of each experiment. The priming fluid consisted of a mixture of 23.2 wt % glycerin, 75.6 wt % water, and 1.2 wt % Triton X-100. The density of the priming fluid matched that of the particles so that the first few particles in the channel did not settle or rise when they mixed with the priming fluid. The surfactant Triton X-100 was added to reduce the presence of bubbles throughout the system.

Procedure

Before each run, the chip and silicone gasket were placed in an ultrasonic bath of deionized water for several minutes. The chip and gasket were then wiped with a clean-room swab to remove residual fibers and dirt from the surfaces. The chip was then blown dry with nitrogen or filtered air. The gasket was placed on the bottom side of the chip and pressed on, starting in the center and working outward. The assembly was then placed on a piece of PMMA and pressed in place to secure it.

The syringes and their attached tubing were weighed empty and then placed in the syringe pump. The gel-loading tip was attached to the entrance of the inlet channel and filled with priming fluid. Priming fluid flowed into the microchannels under the combined actions of capillarity and gravity. If bubbles were present in the channels at this point, the chip was dismantled, cleaned, and reassembled. Each outlet was then connected to tubing that led to a syringe, and the pump was started in withdrawal mode at a high flow rate approximately 100-fold greater than the flow rate used during the experiment. When most of the priming fluid was gone from the gel tip, the flow rates were set to their appropriate values for the experiment and the suspension was added to the tip. Care was taken to ensure that the gel tip remained properly aligned so that the lateral distribution of particle centers was uniform in the inlet channel. After each experiment, the chip was dismantled, sonicated, and cleaned, and the syringes were weighed to determine the flow rates in each branch of the bifurcation during the experiment. The video recording was reviewed and the numbers of particles entering each branch of the bifurcation were counted. Figure 4 shows a video image of particles moving through a Y-shaped bifurcation during the experiment.

Results and Discussion

The downstream branches of each bifurcation are labeled "1" and "2." Because of the symmetry of the Y-shaped bifurcation (Figure 1a), there is no distinction between the two downstream branches, so one of them is arbitrarily selected as branch "1." For the case of an oblique bifurcation (Figure 1b), branch "1" is the downstream branch that is collinear with the inlet branch. The volumetric flow rates in the downstream branches are denoted by Q_1 and Q_2. Because of the low Reynolds number of the flow, particle trajectories in the bifur-

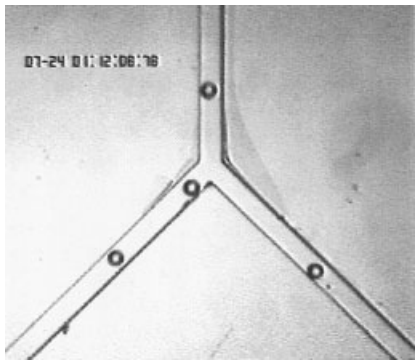

Figure 4. Video image of particles moving through a 100 × 100-μm microfluidic Y-shaped bifurcation with $\lambda = 0.8$ and $\phi = 0.015$.

Flow is in at the top and out through the bottom two branches.

cation are affected only by the ratio Q_1/Q_2, which was fixed by the relative sizes of the two syringes.

For each bifurcation geometry, several runs were made for different combinations of Q_1 and Q_2. After each run, the video recording was reviewed to determine N_1 and N_2, the numbers of particles that entered branches 1 and 2, respectively. The total number of particles that moved through the bifurcation N_T is simply $N_1 + N_2$, whereas the total volumetric flow rate through the bifurcation Q_T is $Q_1 + Q_2$.

To describe the partitioning of particles between the downstream branches for different values of Q_1 and Q_2, it is convenient to report N_1/N_T, the fraction of particles that entered branch 1, as a function of Q_1/Q_T, the fraction of total volume (suspending fluid + particles) that entered that branch.

Additional parameters include the dimensionless particle size λ, which is the ratio of the particle diameter to the channel width and the particle volume fraction ϕ. Given that the particles had diameters of 80 μm, the value of λ is 0.8 based on the 100-μm channel width. The solids volume fraction of the suspension ϕ was 0.015.

Figure 5 shows particle partitioning for two Y-shaped bifurcations that differ in the cross-sectional shapes of the channels composing the bifurcation. Figure 5A pertains to bifurcations composed of square channels (100 × 100 μm) and Figure 5B pertains to bifurcations composed of rectangular channels (100 × 200 μm). The diagonal lines in the figures correspond to hypothetical cases in which the particles and fluid partition identically between the two downstream branches. However, both plots show that N_1/N_T differs from Q_1/Q_T for most values of Q_1/Q_T and that the magnitude of the difference depends on Q_1/Q_T. For Y-shaped bifurcations, particles preferentially enter the downstream branch receiving the greater volumetric flow rate. Furthermore, when the value of Q_1/Q_T exceeds a critical value, say $(Q_1/Q_T)^*$, all of the particles enter that branch ($N_1/N_T = 1.0$) even though some fluid enters the other branch. For the Y-shaped bifurcation composed of square channels (Figure 5A), the value of $(Q_1/Q_T)^*$ is 0.77. The maximum fractional clearance, $1 - (Q_1/Q_T)^*$, indicates the efficiency of the bifurcation flow in separating the particles from liquid. In this case 23% of the fluid was completely cleared of particles in a single pass through the bifurcation.

Comparing the data between Figures 5A and 5B shows that for Y-shaped bifurcations, the channel cross-sectional shape does not strongly affect particle partitioning. The value of $(Q_1/Q_T)^*$ for the rectangular channel, 0.76, differs only slightly from the value for the square cross section.

The major source of uncertainty in the experiment is the syringe pump that drives the flow. The value of Q_1/Q_T was determined by the relative sizes of the two syringes in the pump. However, small variations in the actual flow rates arising from imperfections in the syringe plungers and barrels produce uncertainties in the actual value of Q_1/Q_T. Because N_1/N_T is a strong function of Q_1/Q_T, uncertainties in the flow rate are reflected in variations in the measured values of N_1/N_T for runs with nominally identical values of Q_1/Q_T.

Figure 6 shows particle partitioning for an oblique bifurcation composed of square channels (100 × 100 μm) and an oblique bifurcation composed of rectangular channels (100 × 200 μm). A comparison between Figure 6 and Figure 5 shows that the branching angles strongly affect particle partitioning. Data for the Y-shaped bifurcation were symmetric about the point (0.5, 0.5), which reflects the symmetry of the Y geometry. However, this symmetry of the bifurcation geometry is broken in the oblique case, and the data in Figure 6 are not symmetric about the center of the plot. Instead, the data show that particles prefer branch 1, the branch that is collinear with

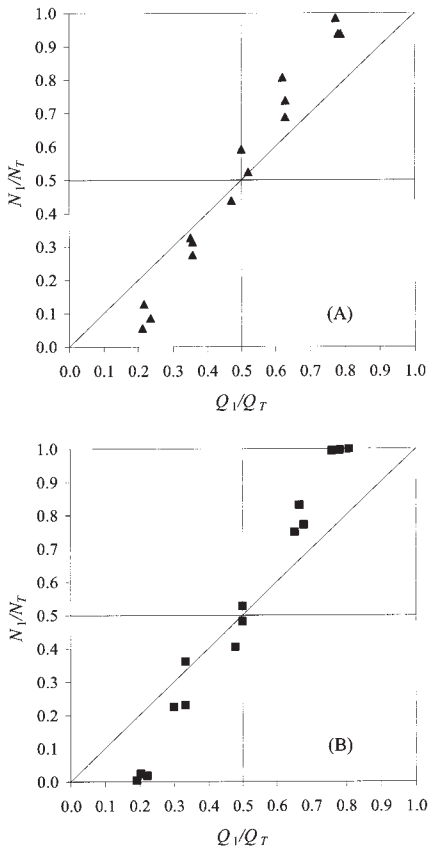

Figure 5. Fraction of particles entering branch 1 as a function of the fraction of total volume entering branch 1 for a 100 × 100-μm Y-shaped bifurcation.

(A, ▲) and a 100 × 200-μm Y-shaped bifurcation (B, ■) with $\lambda = 0.8$ and $\phi = 0.015$.

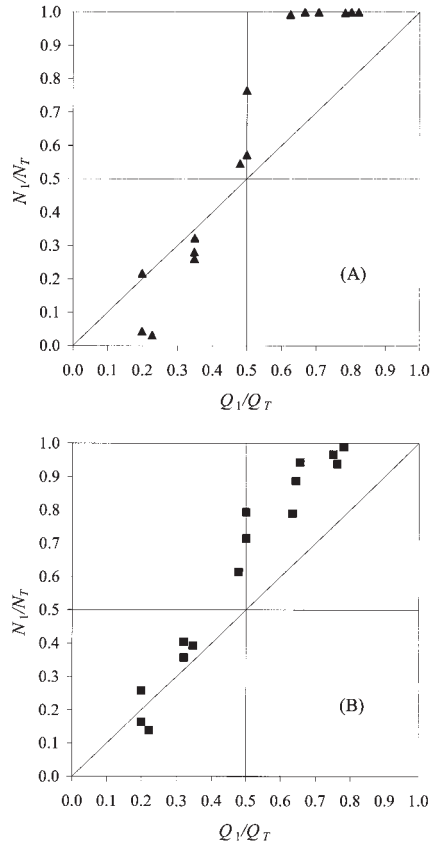

Figure 6. Fraction of particles entering branch 1 as a function of the fraction of total volume entering branch 1 for a 100 × 100-μm oblique bifurcation (A, ▲) and a 100 × 200-μm oblique bifurcation (B, ■) with $\lambda = 0.8$ and $\phi = 0.015$.

the inlet channel. From the perspective of separating the particles from the fluid, the oblique bifurcation is more effective than the Y-shaped bifurcation for most values of Q_1/Q_T. Furthermore, for the bifurcation composed of square channels, the value of $(Q_1/Q_T)^*$ is about 0.63, which means that 37% of the fluid flowing through a single bifurcation is cleared of particles in a single pass. However, data for the oblique bifurcations are sensitive to the dimensions of the channel cross section. The 100 × 100-μm channels show larger values of the fractional particle flux (N_1/N_T) than the 100 × 200-μm channels for $Q_1/Q_T > 0.5$. As the cross-sectional channel area is increased, the effect of hydrodynamic interactions between the wall and the particle diminishes, which, in turn, diminishes the difference between a particle's trajectory and the trajectory of the fluid. The value of $(Q_1/Q_T)^*$ increases to 0.78 for the 100 × 200-μm bifurcation.

Multiple Bifurcations in Series

Microfluidic channels

The experiments described above were designed so that the distribution of particle centers in the inlet branch was uniform across the cross section of the inlet branch, except for layers adjacent to the channel walls where particle centers are excluded. However, experimental observations[12] and numerical calculations[13] have shown that when a particle moves through a bifurcation, its lateral position in the downstream branch is different from its lateral position in the inlet branch. Even if the particles are uniformly distributed across the cross section of the inlet channel, their lateral distributions will be nonuniform in both downstream branches. In the downstream branches of a Y-shaped bifurcation, the particles are skewed toward the inner walls of the bifurcation.[13] A schematic of the distribution of particle centers upstream and downstream of a Y-shaped bifurcation is shown in Figure 7. Fluid near the inner walls of the downstream branches originates near the centerline of the inlet branch. Particles from the central region of the inlet branch are carried by the flow toward the inner walls of the downstream branches. However, fluid near the outer walls of the downstream branches originates near the particle-free layer of the inlet branch. Thus, fluid near the outer walls of the downstream branches is deficient in particles. The issue then becomes whether this nonuniform distribution can be exploited using successive bifurcations to improve the overall effectiveness of a separation.

The multiple-bifurcation system shown in Figure 2 was tested. In this case, the flows from the collinear segments of the downstream bifurcations, segments labeled 2–2 and 3–1 in Figure 2, were combined into a single stream designated as "outlet 1." Flows from the two oblique branches of the downstream bifurcations, segments 2–1 and 3–2, were combined into a single stream designated as "outlet 2." Particle fluxes for the combined streams are reported in the same way that data were reported for single bifurcations.

Data for the multiple bifurcation case are shown in Figure 8. Compared with data for a single bifurcation, data for multiple bifurcations show enhanced particle separation. For most values of Q_1/Q_T, the deviation from the diagonal line is greater in Figure 8 than in Figure 5 or Figure 6. Furthermore, the values

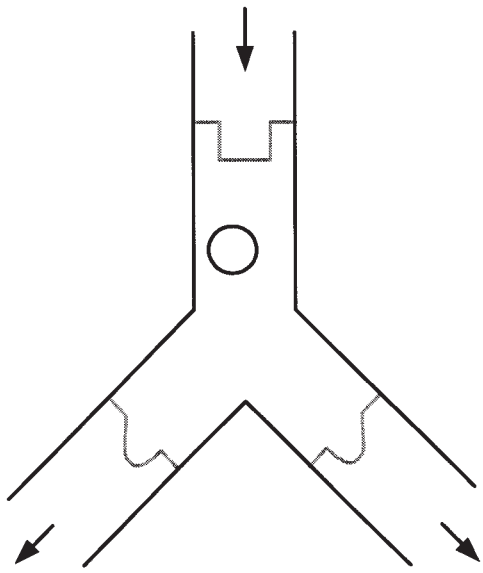

Figure 7. Particle center profiles in upstream (uniform) and downstream branches (nonuniform) of a Y-shaped bifurcation.

Particles lie along the inside walls of the downstream branches after flowing through the bifurcation.

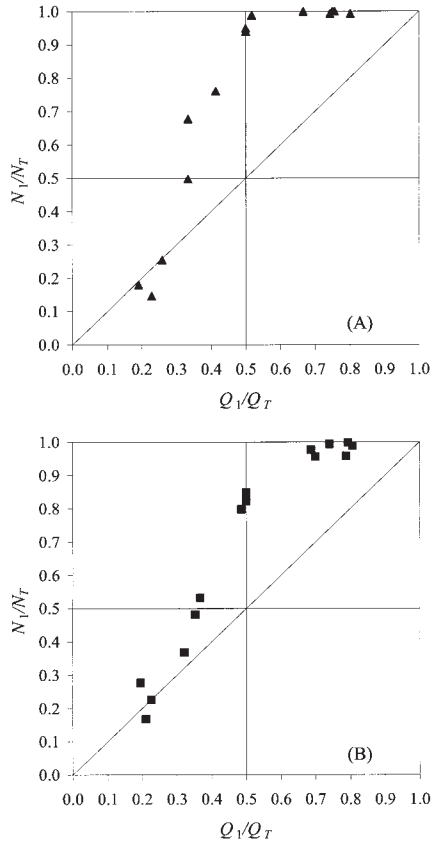

Figure 8. Fraction of particles entering combined outlet 1 as a function of the fraction of total volume entering that outlet for the 100 × 100 μm microfluidic multiple bifurcations (Figure 2) (A, ▲) and the 100 × 200 μm multiple bifurcations (B, ■) with $\lambda = 0.8$ and $\phi = 0.015$.

of $(Q_1/Q_T)^*$, 0.53 for the 100 × 100-μm channels and 0.74 for the 100 × 200-μm channels, are smaller than the corresponding values for single bifurcations.

These results illustrate that the lateral distribution of particles is important in determining particle partitioning in bifurcations that are downstream of other bifurcations. Because the Reynolds number and particle volume fraction are small, there is negligible migration of particles across streamlines in a straight channel. Therefore, when a particle enters the downstream branch of a bifurcation, it maintains the lateral position that it has at the entrance of that branch. Flow through the first bifurcation establishes a nonuniform particle profile in the downstream branches that allows predominantly particle-free fluid to be removed by the second bifurcation. This effect, which occurs in both downstream branches regardless of the partitioning of the flow in the first bifurcation, contributes to the enhanced heterogeneity of particle partitioning overall.

Effects of channel dimensions

Dimensional analysis suggests that the aspect ratio of the channel cross section, and not the absolute channel dimensions, affects particle partitioning. Therefore, it should be possible to separate larger particles using a scaled-up version of the apparatus, provided the Reynolds number remains small. To test this idea, we conducted a series of experiments in a bifurcating rectangular channel that was 1 mm in width and 2 mm in depth. Both dimensions were an order of magnitude larger than those in the microfluidic device. The particles were monodisperse suspensions of spheres (catalog nos. 4375A and 4350A, Duke Scientific) and the suspending fluid was a mixture of 65% Triton X-100 (catalog no. EM-9440, VWR, Chicago, IL) and 35% water. The channels were made by milling matching trenches into two PMMA blocks, which were then bonded together to form the channels. The experimental protocol was analogous to the procedure followed for the microfluidic devices.

Additional details and results are described elsewhere.[17] Here we compare results for the scaled-up device with those for the microfluidic device for one case—the multiple-bifurcation system illustrated in Figure 2. Figure 9 shows particle partitioning in the scaled-up version of the multiple-bifurcation system. As expected, the data qualitatively follow those for the microfluidic version of the multiple-bifurcation geometry with the same channel aspect ratio, which were shown in Figure 8B. In the scaled-up experiment, two particle volume fractions were tested, and the data suggest that volume fraction affects particle partitioning only weakly, at least for volume fractions up to 0.06. The effectiveness of the separation shown in Figure 9 is slightly greater than that shown in Figure 8B for the analogous microfluidic system. This may be attributable to slight imperfections in the channel walls of the microfluidic bifurcations. In any event the major result is that the absolute scale of the device does not significantly affect its usefulness in separating particles, providing the Reynolds number remains small.

Conclusions

We have shown that the partitioning of neutrally buoyant, freely suspended particles at microfluidic bifurcations differs from the partitioning of fluid. The magnitude of the difference depends on the bifurcation geometry and on the aspect ratio of the channel cross section. Using bifurcations in series, we have

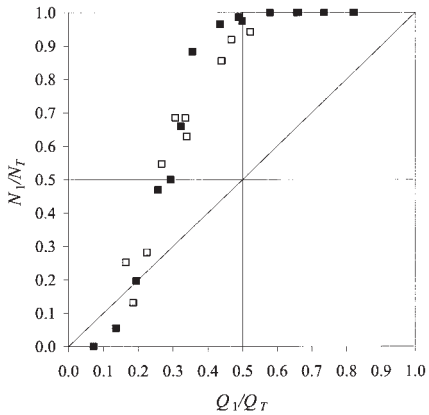

Figure 9. Fraction of particles entering combined outlet 1 as a function of the fraction of total volume entering that outlet for the 1.0 × 2.0-mm slotted multiple bifurcation system (Figure 2) with $\lambda = 0.77$ and $\phi =$ (■) 0.02 and (□) 0.06.

shown that the heterogeneity of particle partitioning can be amplified by taking advantage of nonuniform lateral distributions of particles in downstream branches that result from flow through an upstream bifurcation.

These results can be applied in designing ways of controlling and, if desired, segregating particles or biological cells in complicated microfluidic circuits. By arranging channels and bifurcations in specific ways suggested by results of this study, the distribution of particles among the channels in a circuit can be controlled. In principle, particles can be confined to certain preferred paths and excluded from other paths that may contain sensors, pumps, or other microfluidic components that could by compromised by the particles. Alternatively, the circuit can be arranged to remove particles by concentrating them in a relatively small volume of fluid, and delivering the rest of the fluid, free of particles, for subsequent processing. Such an arrangement would produce, in effect, a kind of "flow-through filter." The important distinction here, though, is that the particles are removed based on hydrodynamics of the low Reynolds number flow, rather than on size exclusion.

The effectiveness of the particle control method described here relies on several essential requirements: the particles must be nondeformable, Brownian motion must be unimportant, the Reynolds number must be small, and the size of the particles must be comparable to the size of the channels. The limitations of the first two requirements have not been tested experimentally. The latter two requirements in effect limit the rate at which particles and fluid can be processed and still maintain control of the particles as described here. To increase throughput, it may be useful to use deep rectangular channels. We showed that the separation effectiveness diminishes only slightly for a 100×200-mm channel. Deeper channels can be made routinely; thus, it should be possible to increase throughput while satisfying requirements for effective control of particle distribution in microfluidic circuits.

The experiments described here provide information about particle partitioning at single bifurcations and small circuits consisting of two bifurcations in series. However, this information can be combined with routine methods of fluidic circuit design, which rely on overall mass and momentum balances, to make more complicated circuits. In this case, the arrangements of the channels dictate local values of the pressure and flow rates that determine, in turn, the partitioning of fluid at bifurcations. Then, it is a straightforward matter to predict the corresponding distribution of particles throughout an entire microfluidic network.

Acknowledgments

This material is based on work supported by the National Science Foundation under Grant CTS-0074788.

Literature Cited

1. Johnson PC. Red cell separation in the mesenteric capillary network. *Am J Physiol.* 1971;221:99-104.
2. Gaehtgens P, Albrecht KH, Kreutz F. Fahraeus effect and cell screening during tube flow of human blood. I. Effect of variation of flow rate. *Biorheology.* 1978;15:147-154.
3. Schmid-Schönbein GW, Skalak R, Usami S, Chien S. Cell distribution in capillary networks. *Microvasc Res.* 1980;19:18-44.
4. Klitzman B, Johnson PC. Capillary network geometry and red cell distribution in hamster cremaster muscle. *Am J Physiol Heart Circ Physiol.* 1982;242:H211-H219.
5. Øfjord ES, Clausen G. Intrarenal flow of microspheres and red blood cells: Skimming in slit and tube models. *Am J Physiol Heart Circ Physiol.* 1983;245:H429-H436.
6. Fenton BM, Carr RT, Cokelet GR. Nonuniform red blood cell distribution in 20 to 100 μm bifurcations. *Microvasc Res.* 1985;29:103-126.
7. Pries AR, Ley K, Claassen M, Gaehtgens P. Red cell distribution at microvascular bifurcations. *Microvasc Res.* 1989;38:81-101.
8. Carr RT, Wickham LL. Influence of vessel diameter on red cell distribution at microvascular bifurcations. *Microvasc Res.* 1991;41:184-196.
9. Enden G, Popel AS. A numerical study of plasma skimming in small vascular bifurcations. *J Biomech Eng.* 1994;116:79-86.
10. Yen RT, Fung YC. Effect of velocity distribution on red cell distribution in capillary blood vessels. *Am J Physiol Heart Circ Physiol.* 1978;235:H251-H257.
11. Ditchfield R, Olbricht WL. Effects of particle concentration on the partitioning of suspensions at small divergent bifurcations. *J Biomech Eng.* 1996;118:287-294.
12. Roberts BW, Olbricht WL. Flow-induced particulate separations. *AIChE J.* 2003;49:2842-2849.
13. Audet DM, Olbricht WL. The motion of model cells at capillary bifurcations. *Microvasc Res.* 1987;33:377-396.
14. Yan ZY, Acrivos A, Weinbaum SA. three-dimensional analysis of plasma skimming at microvascular bifurcations. *Microvasc Res.* 1991;42:17-38.
15. Manga M, Dynamics of drops in branched tubes. *J Fluid Mech.* 1996;315:105-117.
16. El-Kareh AW, Secomb TW. A model for red blood cell motion in bifurcating microvessels. *Int J Multiphase Flow.* 2001;26:1545-1564.
17. Roberts BW. Continuous separations of neutrally buoyant particles using bifurcating channels. PhD Thesis. Ithaca, NY: Cornell University; 2003.

Manuscript received Jun. 9, 2004, and revision received May 18, 2005.